

Roles of secondary electrons and sputtered atoms in ion-beam-induced deposition

Ping Chen,^{a)} Huub W. M. Salemink, and Paul F. A. Alkemade

Kavli Institute of Nanoscience, Delft University of Technology, Lorentzweg 1, 2628 CJ Delft, The Netherlands

(Received 7 July 2009; accepted 3 August 2009; published 2 December 2009)

The authors report the results of investigating two models for ion-beam-induced deposition (IBID). These models describe IBID in terms of the impact of secondary electrons and of sputtered atoms, respectively. The yields of deposition, sputtering, and secondary electron emission, as well as the energy spectra of the secondary electrons were measured *in situ* during IBID using $(\text{CH}_3)_3\text{Pt}(\text{C}_p\text{CH}_3)$ as functions of Ga^+ ion incident angle (0° – 45°) and energy (5–30 keV). The deposition yield and the secondary electron yield have the same angular dependences but very different energy dependences. It was also found that the deposition yield per secondary electron is very high (≥ 10). However, within the investigated angle and energy ranges, the deposition yield is linearly related to the sputtering yield, the offset of which might be due to the contribution of primary ions. They conclude that the sputtered atom model describes IBID better than the secondary electron model. © 2009 American Vacuum Society. [DOI: 10.1116/1.3237147]

I. INTRODUCTION

Ion-beam-induced deposition (IBID) is a direct writing technology in which precursor molecules adsorbed on a substrate surface are decomposed by an ion-beam-induced reaction, resulting in localized material deposition. Owing to its high flexibility with respect to the shape and location of the deposits, IBID is becoming increasingly interesting as a powerful tool for prototyping three-dimensional nanostructures.^{1,2}

A detailed understanding of IBID mechanisms is required to gain full control over the dimensions and composition of the deposits. Generally, IBID is considered a very complex process with possible contributions from primary ions, sputtered atom or ions, secondary electrons (SEs) and thermal spikes.³ Some studies relate IBID to sputtered atom impact and others to secondary electron impact. Dubner *et al.* found that the deposition yield is proportional to the calculated stopping power and, consequently, explained IBID in terms of the energy transfer via a cascade of atom-atom collisions to adsorbed precursor molecules.^{4,5} Chen *et al.* measured different angular dependences of the deposition and sputtering yields, which suggests that IBID cannot be explained solely in terms of ion-solid interactions.⁶ Lipp *et al.* supported the secondary electron model, having observed a linear relationship between the deposition yield and the secondary electron yield within the ion energy range of 10–30 keV.⁷ However, it should be noted that Lipp *et al.* measured the secondary electron yield during ion beam milling instead of during deposition. Chen *et al.* found a charging effect on IBID pillar growth, which suggests that secondary electrons play an important role.⁸ Several other studies also reported contributions from secondary electrons to IBID pillar growth.^{9–11} Hence, it is still unclear whether sputtering or secondary

electron emission is the dominant mechanism in IBID. In this work, we investigate the two IBID models by comparing *in situ* measured yields of deposition, sputtering and secondary electron emission as functions of ion incident angle and energy for a single ion-precursor combination.

II. EXPERIMENT

The experiments were performed in a combined Ga^+ focused ion beam (FIB) and scanning electron microscope (SEM) system (FEI STRATA DualBeam DB235). The metal-organic gas $(\text{CH}_3)_3\text{Pt}(\text{C}_p\text{CH}_3)$ was used as the precursor. The substrates were Si wafers with or without a 30 nm Cu coating layer. The background pressure was 5.5×10^{-7} mbar, and the pressure during growth was 3.3×10^{-6} mbar. A nozzle with a 500 μm diameter opening was located 430 μm above the substrate surface and at an angle of 34° . Patterns were deposited or milled using the Ga^+ FIB with various ion incident angles (0° – 45°) and ion energies (5–30 keV). An ion current density of $0.5 \text{ pA}/\mu\text{m}^2$ was used, corresponding to the current limited growth regime.^{6,12,13} Accordingly, the ion current was 41 pA, the pixel dwell time was 0.2 μs , and the overlap was 0%.

We shall describe the procedure of determining the deposition yield and the sputtering yield during IBID. First, a Pt box was deposited on a Si substrate by means of IBID [Fig. 1(a)]. After the precursor gas supply was switched off, a smaller box was milled by the ion beam inside the deposited box under the same beam conditions. The deposited thickness and the sputtered depth were measured by cross sectioning and subsequent SEM inspection. In order to avoid errors by the rounding of the top edge during sectioning, an electron-beam-induced deposition (EBID) marker layer and an IBID protection layer were deposited on top before sectioning [Fig. 1(b)]. The deposited Pt box was about $10 \times 10 \mu\text{m}^2$ large and was at least 500 nm thick. The resolution of SEM imaging is 1–2 nm. Considering the sharpness

^{a)}Electronic mail: p.chen@tudelft.nl

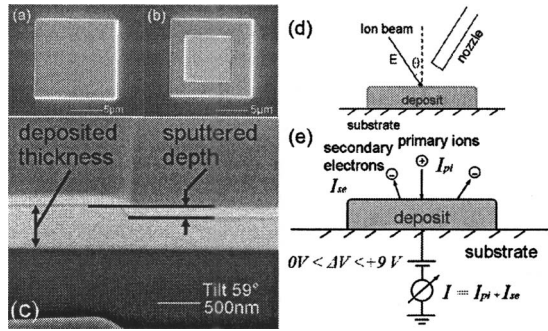


FIG. 1. SEM top views and tilted view of (a) a Pt box grown by means of IBID. (b) The central part is removed by milling with the same FIB settings, then a marker layer is grown via EBID (black layer) plus an IBID protection layer. (c) Cross section. (d) Sketch of the experimental setup with ion incident angle θ and energy E . (e) Measurement of the secondary electron current I_{se} and the energy spectrum of secondary electron with and without a positive bias ΔV .

of the image of the marker layer and of the deposit-substrate boundary as well as the calibration of the SEM, we estimate the error in the yield measurements to be 3%–5%. The composition of the deposits was measured by means of energy dispersive x-ray spectrometry (EDX).

The procedure to determine the yield and the energy spectrum of the secondary electrons during IBID is as follows. The ion current I_{pi} was measured with a Faraday cup. The sample current I during IBID was measured with a picoampere current meter [Fig. 1(d)]. By far most of the sputtered

particles are neutrals,¹⁴ so the contribution of secondary ions to the sample current is negligible. Thus, the secondary electron yield Y_{SE} is $Y_{SE} = (I - I_{pi}) / I_{pi}$. With a positive bias ΔV between the substrate and the current meter, secondary electrons with an energy less than $e \cdot \Delta V$ are attracted back to the substrate, resulting in a reduced sample current I . A shielded box with six 1.5 V batteries was used to apply various biases between 0 and 9 V. Furthermore, the fact that the sample currents measured on bare Si and on Cu-coated Si are the same confirms that the conductivity of Si is sufficiently high to avoid additional sample charging.

III. RESULTS

The sputtering yield is assumed to be the same for bare deposit and the deposit covered by an adsorbed precursor layer. The deposition yield was defined by the measured net deposition yield plus the sputtering yield [Figs. 1(a)–1(c)]. Figure 2(a) shows the angular dependences of the yields of deposition Y_d , sputtering Y_s , and secondary electron emission Y_{SE} for three different ion energies (5, 15, and 30 keV). The deposition yield and the sputtering yield are expressed as volume per incident ion. The angular dependences are normalized at 0° . One sees that the deposition yield has the same angular dependence as the secondary electron yield ($\cos \theta$)^{-1.35}, but a weaker dependence than that of the sputtering yield ($\cos \theta$)^{-2.0}. In Figs. 2(b) and 2(c), the absolute deposition yield is plotted against the absolute yields of secondary electrons and sputtering, respectively. The deposition

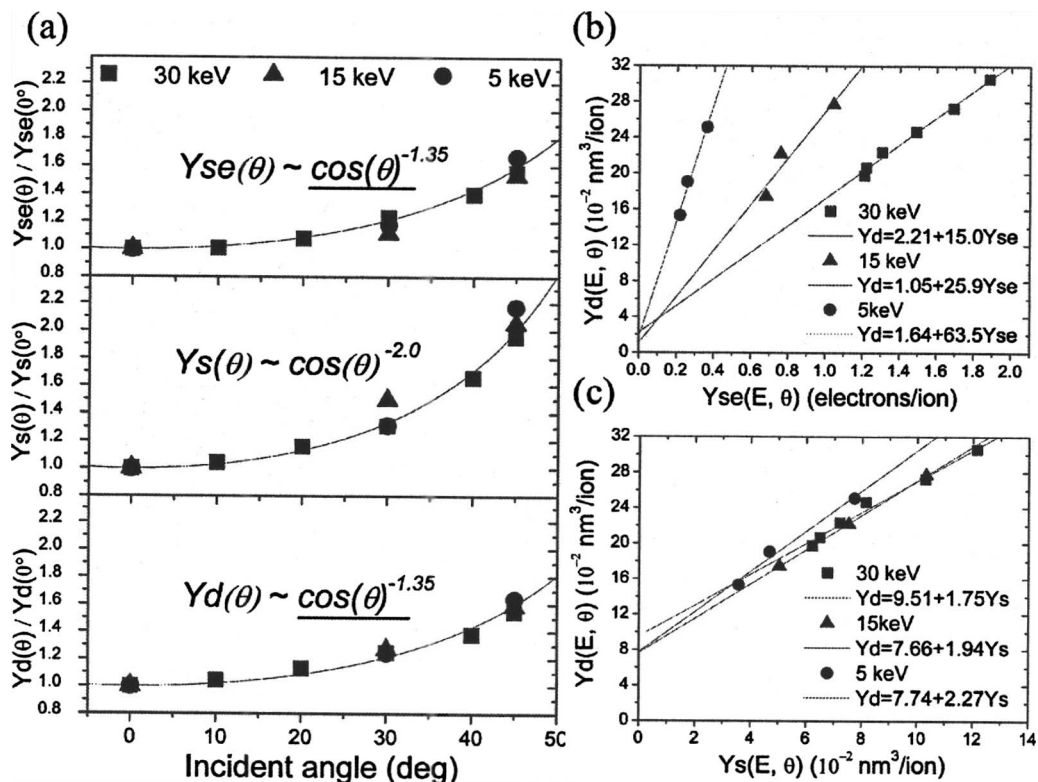


FIG. 2. (a) Normalized secondary electron yield (Y_{SE}), sputtering yield (Y_s), and deposition yield (Y_d) as functions of the ion incident angle θ for three different ion energies E . (b) Correlation between $Y_d(E, \theta)$ and $Y_{SE}(E, \theta)$. (c) Correlation between $Y_d(E, \theta)$ and $Y_s(E, \theta)$.

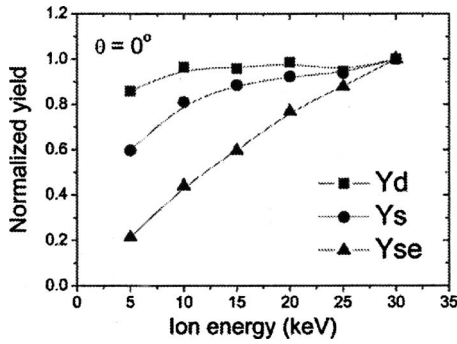


FIG. 3. Normalized secondary electron yield (Y_{SE}), sputtering yield (Y_s), and deposition yield (Y_d) as functions of ion energy E for an ion incident angle θ .

yield varies linearly with the sputtering yield having a slope of about 2.0 and an offset of about $0.09 \text{ nm}^3/\text{ion}$. For constant ion energy, the deposition yield is proportional to the secondary electron yield. According to the EDX analysis, the composition of the deposit is $\text{Ga}_{0.15}\text{Pt}_{0.45}\text{C}_{0.40}$, corresponding to an atomic density of $100 \text{ atoms}/\text{nm}^3$.

The energy dependences of the yields of deposition Y_d , sputtering Y_s , and secondary electron emission Y_{SE} at 0° incidence are given in Fig. 3. They are normalized at 30 keV. The deposition yield decreases by 14%, with ion energy decreasing from 30 to 5 keV. The secondary electron yield decreases by 80%, whereas the sputtering yield decreases by 40%.

Figure 4 presents the energy spectra of secondary electrons in the range from 0 to 9.0 V in steps of 1.5 V. The secondary electron energy shown is the average energy of each energy step. The energy spectra are normalized to the same area. One sees that the energy spectra do not change with the ion incident angle. Furthermore, the lower energy part becomes more dominant with decreasing ion energy.

IV. DISCUSSION

The measured yields of sputtering, deposition, and secondary electron emission increase with increasing incident angle and ion energy. These results are consistent with previous experimental^{15,16} and theoretical¹⁷ works on sputtering, deposition,^{18,19} and secondary electron emission.²⁰⁻²² More-

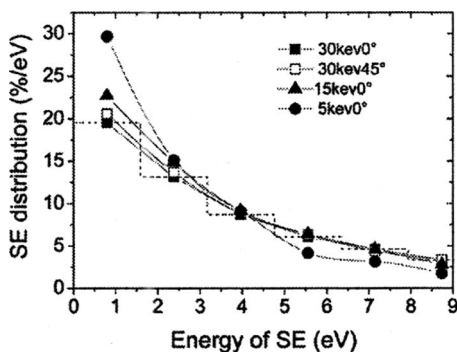


FIG. 4. Observed energy spectra of secondary electrons (SEs) during IBID for different ion incident angles and ion energies.

over, the energy spectrum of the secondary electrons shifts slightly to higher energies with increasing ion energy, consistent with related studies.^{22,23} Here we will discuss our experimental results in light of the two models for IBID: the sputtered atom (atom-atom collision cascade) model^{4,5} and the secondary electron model.⁷

We have observed a strong correlation between deposition and secondary electron emission: both exhibit the same dependence on ion incident angle. However, without detailed knowledge of the transport and interactions of primary ions, secondary atoms, and secondary electrons, one cannot rule out the possibility that this observed proportionality is purely circumstantial. The proportionality between deposition yield and secondary electron emission depends strongly on the ion energy. For a density of $100 \text{ atoms}/\text{nm}^3$, several tens of precursor molecules are decomposed per secondary electron. This number is very high. If the secondary electron model for IBID is valid, secondary electrons must be more efficient in decomposing precursor molecules at low ion energies than at high ion energies. The measured difference is a factor of 4 between 5 and 30 keV ions [Fig. 2(b)]. If true, the higher efficiency must be caused by the different characteristics of the secondary electrons plus the different responses of the precursor molecules to these different types of secondary electrons. Important characteristics are the angular and energy distributions of the emitted electrons. The measured energy spectra of the secondary electrons are indeed different, but the difference is small. Furthermore, decomposition in EBID is obviously caused by electrons, either primary or secondary (excluding decomposition by a thermal spike). Thus, if the secondary electron model is valid for IBID, strong similarities between EBID and IBID must exist. Little is known about precursor decomposition in EBID except that it depends on the primary or secondary electron energy.²⁴⁻²⁶ Even if one assumes that only the very low-energy secondary electrons ($<1.5 \text{ eV}$) decompose precursor molecules in EBID and IBID, their slightly higher relative intensity in our study (a factor of ~ 1.5 at 5 keV compared to 30 keV) is insufficient to explain the four times higher efficiency observed. Therefore we conclude that the high deposition yield per secondary electron and its strong ion energy dependence are evidence against the validity of the secondary electron model for IBID.

The deposition yield and the sputtering yield have different angular dependences. However, all our data plotted together display a linear relationship between deposition and sputtering [Fig. 2(c)], independent of incidence angle and ion energy. Extrapolation of the measured relationship suggests that within the limit of no sputtering, deposition is still possible. Either there is a threshold for sputtering or there is an energy-independent mechanism for precursor decomposition. One might explain this offset by the stronger bonds of Pt atoms in the deposit than in the adsorbed precursor layer. Alternatively, it is possible that the decomposition by primary ions causes the offset. Dubner *et al.* reported that the deposition yield is proportional to the nuclear stopping

power.^{4,5} However, we note that a linear relationship with an offset between deposition and sputtering can also be found in their work (Table II in Ref. 4).

In summary, our data show that the mechanism for IBID is more likely to be sputtering than secondary electron emission.

V. CONCLUSIONS

The similar angular dependences of the deposition yield and the secondary electron yield support the secondary electron model. However, the very different energy dependence and the high deposition yield (tens of atoms) per secondary electron contradict this model. The deposition yield correlates linearly to the sputtering yield with an offset that is independent of the incident angle and the ion energy. The offset could be due to decomposition by primary ions. It will be interesting to investigate conditions where deposition is possible without concurrent sputtering. From these observations we conclude that the sputtered atom model is more likely than the secondary electron model to be the dominant mechanism in IBID. A more detailed quantitative discussion will require additional experimental data, theory, and modeling, but that is beyond the scope of the present paper.

ACKNOWLEDGMENTS

The authors thank Emile van der Drift and Vadim Sidorkin (both at Delft University of Technology) for their helpful discussions. They also gratefully acknowledge financial support by NanoNed.

¹A. Wagner, J. L. Mauer, P. G. Blauner, S. J. Kirch, and P. Longo, *J. Vac. Sci. Technol. B* **8**, 1557 (1990).

²S. Matsui, T. Kaito, J. Fujita, M. Komuro, and K. Kanda, *J. Vac. Sci. Technol. B* **18**, 3181 (2000).

³G. M. Shedd, H. Lezec, A. D. Dubner, and J. Melngailis, *Appl. Phys. Lett.* **49**, 1584 (1986).

⁴A. D. Dubner, A. Wagner, J. Melngailis, and C. V. Thompson, *J. Appl. Phys.* **70**, 665 (1991).

⁵J. S. Ro, C. V. Thompson, and J. Melngailis, *J. Vac. Sci. Technol. B* **12**, 73 (1994).

⁶P. Chen, P. F. A. Alkemade, and H. W. M. Salemink, *Jpn. J. Appl. Phys., Part 1* **47**, 5123 (2008).

⁷S. Lipp, L. Frey, C. Lehrer, E. Demm, S. Pauthner, and H. Ryssel, *Microelectron. Reliab.* **36**, 1779 (1996).

⁸P. Chen, H. W. M. Salemink, and P. F. A. Alkemade, *Jpn. J. Appl. Phys., Part 1* **47**, 8120 (2008).

⁹J. Fujita, M. Ishida, T. Ichihashi, T. Sakamoto, Y. Ochiai, T. Kaito, and S. Matsui, *Jpn. J. Appl. Phys., Part 1* **41**, 4423 (2002).

¹⁰J. Fujita, M. Ishida, T. Ichihashi, Y. Ochiai, T. Kaito, and S. Matsui, *J. Vac. Sci. Technol. B* **20**, 2686 (2002).

¹¹J. Fujita, M. Ishida, T. Ichihashi, Y. Ochiai, T. Kaito, and S. Matsui, *J. Vac. Sci. Technol. B* **21**, 2990 (2003).

¹²A. D. Dubner and A. Wagner, *J. Appl. Phys.* **65**, 3636 (1989).

¹³T. P. Chiang, H. H. Sawin, and C. V. Thompson, *J. Vac. Sci. Technol. A* **15**, 3104 (1997).

¹⁴J. Orloff, M. Utlaut, and L. Swanson, *High Resolution Focused Ion Beams: FIB and Its Applications* (Kluwer Academic, New York/Plenum, New York, 2003), Chap. 4.

¹⁵H. H. Anderson and H. L. Bay, in *Sputtering by Particle Bombardment I*, edited by R. Behrisch (Spring, Berlin, 1981), p. 145.

¹⁶A. Benninghoven, F. G. Rüdenauer, and H. W. Werner, *Secondary Ion Mass Spectrometry* (Wiley, New York, 1987), p. 699.

¹⁷P. Sigmund, in *Sputtering by Particle Bombardment I*, edited by R. Behrisch (Spring, Berlin, 1981), p. 9.

¹⁸R. M. Langford, *Microelectron. Eng.* **84**, 784 (2007).

¹⁹J. M. De Teresa, R. Córdoba, A. Fernández-Pacheco, O. Montero, P. Strichovanec, and M. R. Ibarra, *J. Nanomater.* **2009**, 936863 (2009).

²⁰J. L. H. Jonker, *Philips Res. Rep.* **6**, 372 (1951).

²¹H. J. Klein, *Z. Phys.* **188**, 78 (1965).

²²B. A. Brusilovsky, *Appl. Phys. A: Solids Surf.* **50**, 111 (1990).

²³M. E. Rudd, *Phys. Rev. A* **20**, 787 (1979).

²⁴I. Utke, P. Hoffmann, and J. Melngailis, *J. Vac. Sci. Technol. B* **26**, 1197 (2008).

²⁵P. C. Cosby, *J. Chem. Phys.* **98**, 7804 (1993).

²⁶H. F. Winters and M. Inokuti, *Phys. Rev. A* **25**, 1420 (1982).